International Journal of Control, Automation and Systems 15(1) (2017) 329-344
http://dx.doi.org/10.1007/s12555-014-0363-2
ISSN:1598-6446 eISSN:2005-4092
http://www.springer.com/12555

Robust Model Predictive Control of Biped Robots with Adaptive On-line Gait Generation

Reza Heydari and Mohammad Farrokhi*

Abstract: In this paper, an on-line gait control scheme is proposed for the biped robots for walking up and down the stairs. In the proposed strategy, the nonlinear model predictive control approach is used for the trajectory planning and as well as for the control of the robot. The motion of the robot is expressed in the form of a cost function and some constraints that are related to the stable walking of the robot. The main feature of this method is that it does not need any off-line trajectory planning and the walking gait is formulated such that the environmental and stability constraints of the robot are satisfied. This on-line trajectory planning gives the important ability to the robot to adjust its gait lengths. In this way, the robot is able to ascend and descend the stairs without knowing the height and depth of the stairs in advance. In the control algorithm, the Radial-Basis Function (RBF) neural network with on-line training method is used to model the behavior of the robot over the prediction horizon. The stability analysis of the closed-loop system is performed using the Lyapunov method as well as the Poincaré map. The proposed method is applied to a 5-DOF biped robot in the sagittal plane. The simulation results show effectiveness of the proposed method.

Keywords: Biped robot, model predictive control, neural network, Poincaré map.

1. INTRODUCTION

One of the great challenges for the biped robots is walking in uneven terrains, such as inclined surfaces and stairs. Despite wheeled robots, biped robots have a better ability to move on uneven grounds or other complex environments. On the other hand, the dynamics of these robots are complex and inherently unstable. Therefore, selecting an effective control scheme for ensuring the stability of the robot during walking is very vital. Many researchers proposed the trajectory generation and control algorithm for the biped robots on flat surfaces [1–3]. However, there exist a few studies about the ascending/ descending stairs by these robots [4–6].

During motion, it is necessary that the robot stay balanced. One of the stability criteria for stable walking of the biped robots is the Zero Moment Point (ZMP) [7, 8], which is defined as the point on the ground where the sum of all the moments of active force acting on the biped robot is equal to zero. When the ZMP falls within the polygon of the support area, the walking is defined to be dynamically stable [9]. In the case of single support phase, the support polygon is the area of the stance foot on the ground whereas for the double support phase, it is the area containing both feet touching the ground.

Park *et al.* have presented a trajectory generation method and control approach for a biped robot to climb stairs [5]. In their method, the path planning is performed off-line using the Virtual Height Inverted Pendulum Mode (VHIPM) method. The motion of the Center of the Mass (COM) is modeled by the variable length pendulum mode. In this way, the ZMP error can be reduced via adjustment of the pendulum length. First, the desired ZMP trajectory is designed. Then, the Center of Gravity (COG) trajectory in the x and y directions is designed based on the desired ZMP trajectories. The COG trajectory in the z direction is generated using a sixth order polynomial. Fu et al. have proposed a method for walking control of humanoid robot while climbing stairs [10]. This approach consists of a stair-climbing gait and a sensory control strategy. The sensory control strategy consists of a torso attitude controller, a ZMP compensator, and an impact reducer. The feedback control parameters are adjusted by a reinforcement learning method.

Almost all methods presented in literature are designed based on a predefined path tracking. However, when the environment changes, it is necessary to redesign the trajectory. Nevertheless, human does not walk based on a predefined trajectory. He satisfies some motion constraints such as stability, avoiding collision with the obstacles, and

Manuscript received September 18, 2014; revised March 7, 2015 and June 28, 2015; accepted December 28, 2015. Recommended by Associate Editor Seul Jung under the direction of Editor Hyouk Ryeol Choi.

Reza Heydari and Mohammad Farrokhi are with the Department of Electrical Engineering Iran University of Science and Technology, Narmak, Farjam St, Tehran 16846-13114, Iran (e-mails: farrokhi@iust.ac.ir, reza_heydari1988@yahoo.com).
* Corresponding author.

minimizing the energy consumption. Moreover, if there are some errors in the path tracking, it does not create a serious problem in the robots motion as long as the constraints are satisfied. In other words, human predicts his next steps based on these constraints and not a predefined path. One of the appropriate control schemes to fulfill these goals is the Model Predictive Control (MPC) methods. In [11], the Nonlinear MPC (NMPC) method is used for the on-line trajectory generation and control of a 7-DOF biped robot when it walks on flat surfaces. The main feature of their method is using an on-line iterative optimization approach to compute the decision variables over the prediction horizon. Moreover, the predictive controller uses the dynamic model of the biped robot to predict its future behavior. Therefore, if there is any uncertainty in the robot, the controller may not work well. Diedam et al. have used MPC method for the HRP-2 humanoid robot [12]. In their method, the trajectory generation and control of the robot is performed simultaneously. They have used the MPC controller to track the desired ZMP. In their method, the desire ZMP trajectory is generated off-line and the cost function is defined as the error between the real and desired ZMP. In [13], implementation of MPC for the real-time walking pattern generation of a humanoid robot is presented. The nonlinear dynamic model of the robot is approximated using a linear discrete-time system. It is well known that in the presence of linear constraints on the input and output, the MPC problem can be set up as a quadratic programming. Hence, at each step, a quadratic function is solved. In [14], the NMPC with the Nonlinear Disturbance Observer (NDO) has been employed in order to reject the parameter uncertainties and the external forces acting on the robot. The NMPC is designed in such a way that the gait length may be changed in the presence of disturbances to maintain the robots stability. Wieber has used the MPC for the stable walking of a biped robot on flat surfaces [15]. In order to reduce the complexity of the problem, simplified equations of the inverted pendulum is used instead of the dynamic equation of biped robots.

In the past two decades, several studies have been presented on the modeling, analysis and control of the biped robots. Due to the high nonlinearity of these robots, the stability analysis usually is performed based on a linear model of the system [16–18]. However, the linear model can be used as long as the states of the system are near the operating point. For this reason, the linear model can be used only for stability analysis around the operating point. In recent years, researchers have used the Poincaré map for stability analysis of the biped robots. Considering that walking of the biped robot is a repetitive motion, the Poincaré map is a suitable approach for the study of these systems [19–21]. The closed-loop system is stable if all eigenvalues of the linearized Poincaré map are inside the unit circle [22].

This paper employs the NMPC method for simultaneous trajectory generation and control of biped robots for ascending and descending the stairs. In the proposed strategy, the gait length is adjusted to satisfy the stability, the environment constraints, and the cost function. Using the NPMC to adjust the gait length, it provides more flexibility and improves the ability of the controller to maintain stability of the biped robot in the complex environments. In other words, the robot can successfully ascend and descend the stairs with different heights and depths. To achieve these goals, it is necessary to define the cost function and the constraints properly. Moreover, the important issue that arises in the application of the MPC is that the performance of the controller depends on the prediction model. For this reason, the prediction model should adapt itself to the changes in the robot and in the environment. In this paper, the Radial-Basis Function (RBF) Neural Network (NN) is used to identify adaptively the biped robot. In this way, the performance of the controller in the presence of uncertainties and disturbances is greatly improved. The stability analysis of the closed-loop system is performed using the Lyapunov stability method as well as the Poincaré map.

2. DYNAMIC OF BIPED ROBOT

The schematic diagram of the biped robot with five-DOF that is used in this paper is shown in Fig. 1. The biped robot consists of a torso and two legs. The torso of the robot is connected to the hip via a rotational joint. There is an actuator at each joint of the robot. Therefore, the system is fully actuated. It is assumed that the feet are massless. Moreover, it is assumed that the feet are always parallel to the ground. In addition, it is assumed that the friction between the feet and the ground is sufficiently large to ensure no slipping of the stance leg. Each gait of the robot is composed of three phases: 1) Single Support Phase (SSP), 2) Double Support Phase (DSP) and 3) SSP impact. The differential equation of the dynamic motion of the robot in each phase can be derived using the Lagrangian method or the Newton-Euler formulation.

2.1. Single support phase (SSP)

In this phase, one foot of the robot is in contact with the ground and the other foot swing from the rear to the front. Moreover, the tip of the stance leg is fixed on the ground. The dynamic equation describing the robots motion in the SSP can be written as follows:

$$\mathbf{D}(\boldsymbol{\theta})\ddot{\boldsymbol{\theta}} + \mathbf{H}(\boldsymbol{\theta},\dot{\boldsymbol{\theta}})\dot{\boldsymbol{\theta}} + \mathbf{G}(\boldsymbol{\theta}) = \boldsymbol{\tau}, \tag{1}$$

where $\mathbf{D}(\boldsymbol{\theta})$ is a 5×5 positive definite and symmetric inertia matrix, $\mathbf{H}(\boldsymbol{\theta},\dot{\boldsymbol{\theta}})$ is a 5×5 matrix of centrifugal and Coriolis terms, and $\mathbf{G}(\boldsymbol{\theta})$ is a 5×1 vector of gravity terms. Moreover, $\boldsymbol{\theta}$, $\dot{\boldsymbol{\theta}}$, $\ddot{\boldsymbol{\theta}}$ and $\boldsymbol{\tau}$ are the vector of generalized

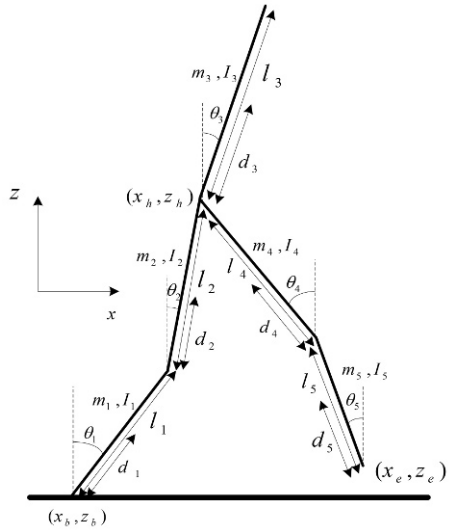

Fig. 1. Five-link biped robot in the sagittal plane.

cordinates, velocities, accelerations, and torques, respectively. The elements of $\mathbf{D}(\boldsymbol{\theta})$, $\mathbf{H}(\boldsymbol{\theta},\dot{\boldsymbol{\theta}})$ and $\mathbf{G}(\boldsymbol{\theta})$ for a 5-DOF biped robot are given in [23].

2.2. Double support phase (DSP)

In the DSP, both feet are in contact with the ground while the body can move forward slightly. This phase begins when the tip of swing leg contacts the ground and terminates with the tip of the rear leg taking off the ground. Since both feet are fixed on the ground during this phase, there exist a set of holonomic constraint equations as [23]

$$\boldsymbol{\Phi} = \begin{bmatrix} x_e - x_b - L \\ y_e - y_b \end{bmatrix} = \mathbf{0}, \tag{2}$$

where L is the distance between the tips of the two feet, which is constant in every step, (x_e, y_e) and (x_b, y_b) are the coordinate of the tip of the swing leg and the stance leg, respectively. The dynamic equation of the biped robot in the DSP can be written as

$$\mathbf{D}(\boldsymbol{\theta})\ddot{\boldsymbol{\theta}} + \mathbf{H}(\boldsymbol{\theta},\dot{\boldsymbol{\theta}})\dot{\boldsymbol{\theta}} + \mathbf{G}(\boldsymbol{\theta}) = \mathbf{J}^T(\boldsymbol{\theta})\boldsymbol{\lambda} + \boldsymbol{\tau}, \tag{3}$$

where $\mathbf{D}$, $\mathbf{H}$, $\mathbf{G}$ and $\boldsymbol{\tau}$ are the same as in (1), $\boldsymbol{\lambda}$ is a 2×1 vector of the Lagrange multipliers, and $\mathbf{J}$ is a 2×5 Jacobean matrix.

2.3. Impact effect

At the time when the tip of the swing leg collides with the ground, the angle velocities change discontinuously. Then, the swing leg becomes the support leg and the support leg leaves the ground and becomes the swing leg. The interval of exchange of legs during the impact is assumed infinitely small and a perfectly plastic collision take place, which means that the tip of the swing leg does not leave the walking surface after the impact. During the impact phase, no change in the joint angular positions is assumed. The instantaneous change in the joint angular velocities of the links can be described as [23]

$$\dot{\boldsymbol{\theta}}^+ = \dot{\boldsymbol{\theta}}^- + \mathbf{D}^{-1}\mathbf{J}^T(\mathbf{J}\mathbf{D}^{-1}\mathbf{J}^T)^{-1}(-\mathbf{J}\dot{\boldsymbol{\theta}}^-), \tag{4}$$

where $\dot{\boldsymbol{\theta}}^+$ and $\dot{\boldsymbol{\theta}}^-$ are 5×1 angular velocity right after and before the impact, respectively.

3. NONLINEAR MODEL PREDICTIVE CONTROL

The Model Predictive Control (MPC) is one of the most successful control strategies. The MPC is an optimization-based control concept that can be applied to a wide range of dynamic systems. In this method, the main idea to find a control law for the system is to optimize the predicted future behavior of the system. One of the major advantages of the MPC is that the constraints imposed on the system can be incorporated into the control law. The MPC generates the control actions by optimizing an objective function repeatedly over a finite moving prediction horizon using the system constraints based on a model of the dynamic system.

3.1. Cost function

The distance of the ZMP from the boundaries of the support polygon can be considered as a criterion for the stability of the biped robot. Therefore, if the ZMP is set at the middle of the support polygon, the biped robot has the best stability margin. On the other hand, when the ZMP is close the boundaries of the support polygon, the stability of the system is marginal and when the ZMP leaves the support polygon, the system becomes unstable. Hence, the cost function can be defined as the ZMP distance from the boundaries of the support polygon. Moreover, in order to optimize the energy consumption, the biped robot must be able to perform the control objectives with the least expenditure control inputs. To achieve this aim, the expression of the consumption energy should be considered in the cost function. Therefore, the cost function in the predictive control for the SSP and DSP is defined as

$$C(k) = \sum_{j=1}^{N_p} Q\left(\frac{e^{D_{ZMP}(k+j|k)} - e^{D_{ZMP_{\min}}}}{e^{D_{ZMP_{\max}}} - e^{D_{ZMP_{\min}}}}\right) + \sum_{j=1}^{N_c} \boldsymbol{\tau}^T(k+j|k)\mathbf{R}\boldsymbol{\tau}(k+j|l), \tag{5}$$

where

$$D_{ZMP} = \left|\frac{w}{2} - x_{ZMP}\right|, \tag{6}$$

in which w and D_{ZMP} are the foot length and the ZMP error (i.e., the ZMP distance from the boundaries of the support polygon), respectively, $\mathbf{R}$ is a positive definite and constant matrix and Q is a positive and constant coefficient,

$[D_{ZMP_{\min}}, D_{ZMP_{\max}}]$ is the interval variation of the ZMP error, N_p and N_c are the prediction and control horizons, respectively, x_{ZMP} is the horizontal position of the ZMP, and $\boldsymbol{\tau}$ is the torque vector. Moreover, the notation $\boldsymbol{\tau}(k+j|k)$ indicates the value of $\boldsymbol{\tau}$ at instant $k+j$ predicted at instant k.

3.2. Constraints

As it was previously mentioned, in the proposed method in this paper, no predefined path is defined for the biped robot and the trajectory generation is performed on-line. The ascending and descending stairs and their restrictions can be expressed in the form of a set of constraints. Therefore, different constraints should be defined for each phase of the walking. These are explained in the followings.

3.2.1 DSP constraints

In this phase, both legs are on the ground and the robots body moves forward slowly. For this phase, the physical, motion and energy optimization constraints are defined as follows:

1) The joint variables are bounded by the lower and upper limits as

$$\theta_{i_{\min}} \leq \theta_i \leq \theta_{i_{\max}} \qquad (i = 1,2,4,5). \tag{7}$$

2) Since the biped robot is a mobile robot, it is difficult to provide high torques to the joints. Therefore, the controller must comply with the limitations of the actuators. Moreover, from the practical point of view, the control inputs are in a pre-specified range. Hence,

$$\tau_{i_{\min}} \leq \tau_i \leq \tau_{i_{\max}} \qquad (i = 1,2,...,5). \tag{8}$$

3) The biped robot must move only forward, which requires that the horizontal speed of the center of the mass (COM) must be positive

$$\dot{x}_{COM} \geq 0. \tag{9}$$

4) From the view point of the natural human walking, it is desired that the torso is kept directly upward or oscillates slightly around the upright position

$$\theta_{\min} \leq \theta_3 \leq \theta_{\max}. \tag{10}$$

5) One desired feature of the biped gait in DSP is to minimize the vertical oscillation of the gravity center, which requires to minimize the vertical motion of the hip joint

$$y_{h_{\min}} \leq y_h \leq y_{h_{\max}}. \tag{11}$$

3.2.2 SSP constraints

During the SSP, the free end of the swing leg is in forward motion, moving from the back of the body towards front of it. It should be mentioned that the free end of the swing leg does not follow through a symmetric path when ascending or descending stairs.

For a smooth and natural walking in this phase, it is necessary to satisfy the following constraints:

1) The first four constraints are similar to the DSP constraints.

2) The horizontal velocity of the free end of the swing leg must satisfy the following constraint:

$$\begin{cases} \dot{x}_e \geq \beta_{\min} \dot{x}_{COM} \sin\left(\dfrac{y_e - y_0}{2(H_m - y_0)}\pi\right), \\ \dot{x}_e \leq \beta_{\max} \dot{x}_{COM} \sin\left(\dfrac{y_e - y_0}{2(H_m - y_0)}\pi\right), \end{cases} \tag{12}$$

where $\dot{x}_e$ and $\dot{x}_{COM}$ are the horizontal velocity of the tip of the swing leg and the center of the mass, respectively. and H_m is the maximum height of the tip of the swing leg relative to the stance leg. In the first part of the motion, y_0 is equal to the height of the first stair and in the second part, it is equal to the height of the destination stair. Moreover, x_e and y_e are the horizontal and vertical position of the tip of the swing leg, respectively, $\beta_{\min}$ and $\beta_{\max}$ and are the designing parameters.

3) Based on the diagram in Fig. 2, during the taking off, the vertical velocity of the free end of the swing leg should be positive and during landing it should be negetive and adapt to the robot COM velocity.

$$\begin{cases} \dot{y}_e \geq \delta \sin(|x_e - x_b|\pi) \sin\left(\dfrac{y_e - y_0}{2(H_m - y_0)}\pi\right), & x_e \leq x_b, \\ \dot{y}_e \leq \delta \sin(|x_e - x_b|\pi) \sin\left(\dfrac{y_e - y_0}{2(H_m - y_0)}\pi\right), & x_e \geq x_b, \end{cases} \tag{13}$$

where x_b and y_e are the horizontal position of the stance leg and the vertical velocity of the tip of the swing leg, respectively, and δ is a designing parameter. It can be observed from (13) that when the tip of the swing leg contacts the ground, the velocity is zero, which leads to a softer impact.

4) During the stairs climbing, the swing leg may hit the edge of the stair (Fig. 3). To solve this problem, the following constraint should be satisfied:

$$\text{IF } y_e \leq y_{\text{edge}} \text{ THEN } d > 0, \tag{14}$$

where y_{edge} and d are shown in Fig. 2.

5) During descending the stairs, in order to avoid collision of the tip of the swing leg with the edge of the front step (Fig. 3), the following constraint should be satisfied:

$$\text{IF } x_{diff} \geq 0 \text{ THEN } r > 0, \tag{15}$$

where x_{diff} and r are shown in Fig. 3.

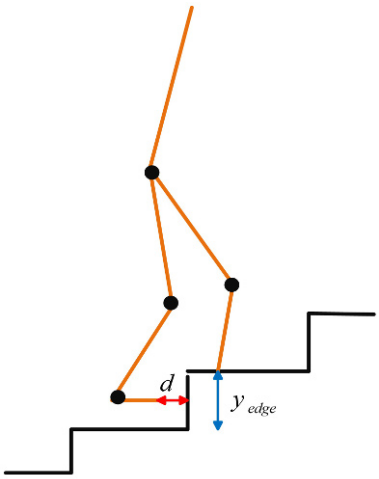

Fig. 2. Constraint on the swing leg in ascending stairs.

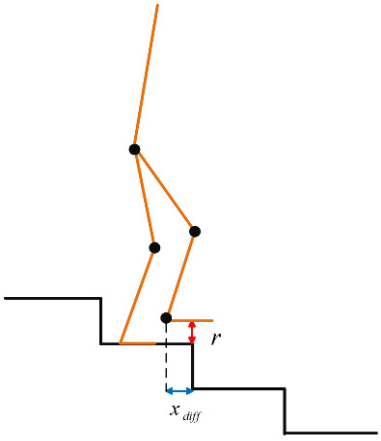

Fig. 3. Constraint on the swing leg in descending stairs.

4. IDENTIFICATION OF DYNAMIC MODEL

The MPC performance greatly depends on the system model. However, in practical applications, accurate modeling using the exact analytical methods is impractical, especially for complex nonlinear systems such as the biped robots. Moreover, when there are some parameter uncertainties in the robot or the structure of the prediction model is different from that of the real biped robot, the robot may become unstable. Hence, in order to cope with these issues, it is necessary to use an adaptive mechanism to identify the systems parameters. It is well known that Neural Networks (NNs) are universal approximators. That is, NNs can be used to approximate any nonlinear function with desired accuracy. In this paper, Radial-Basis Function (RBF) NNs are used to identify adaptively the model of the biped robot. In this way, the MPC controller becomes robust against changes in the system and the environment. To predict the outputs of the robot over the prediction horizon, a cascade of RBFNNs are used. This means that the output of the NN at each step is used as input to the next NN (Fig. 4).

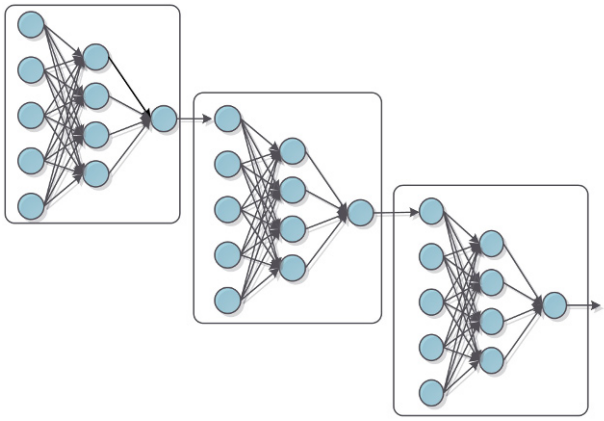

Fig. 4. Cascade of NNs to predict the outputs of system over the prediction horizon.

In the control strategy, one RBFNN is used to predict the position or velocity of each joint of the robot. Therefore, two NNs are designated for every joint of the robot. Hence, 10 NNs are needed for a 5 DOF robot. The inputs to every NN are the angular position and velocity of all five joints and the torque of the corresponding joint at the current sampling time. The output of the NN is the predicted angular position or velocity of the corresponding joint at the next sampling time. Since the biped robot is inherently an unstable system, the NNs might require some mild off-line training in order to become familiar with the behavior of the robot when working on-line.

The structure of a typical RBFNN is shown as Fig. 5, where $\mathbf{x} = [x_1, x_2, ..., x_n]^T$ is the input vector. Assuming there are m neurons in the hidden layer, the value of the Gaussian function h_j for the jth neuron can be obtained as

$$h_j = \exp\left(-\frac{\|\mathbf{x} - \mathbf{c}_j\|}{2b_j^2}\right), \quad j = 1, 2, ..., m, \tag{16}$$

where $\mathbf{c}_j = [c_{j1}, c_{j2}, ..., x_{jn}]^T$ is the center of the jth neuron in m-dimensional space, and $b_j > 0$ represents the width of the Gaussian function.

The output of the RBFNN is the weighted sum of the Gaussian function

$$y_{\text{RBF}} = w_1 h_1 + w_2 h_2 + \cdots + w_m h_m, \tag{17}$$

where $\mathbf{w} = [w_1, w_2, ..., w_m]^T$ is weight vector. To train the network parameters using the gradient descent algorithm, the following instantaneous performance index is defined first:

$$E(k) = \frac{1}{2}(y(k) - y_{\text{RBF}}(k))^2. \tag{18}$$

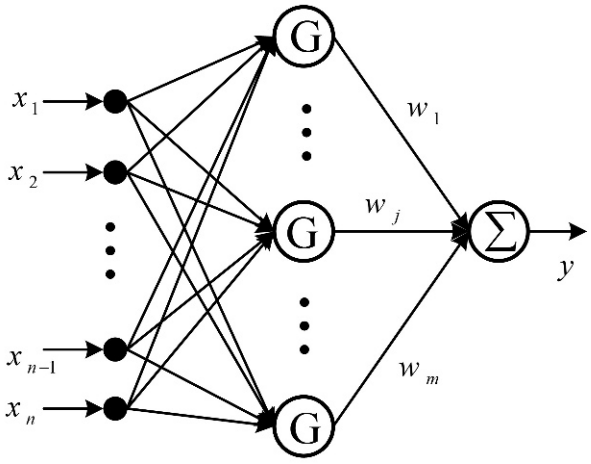

Fig. 5. The structure of a typical RBFNN.

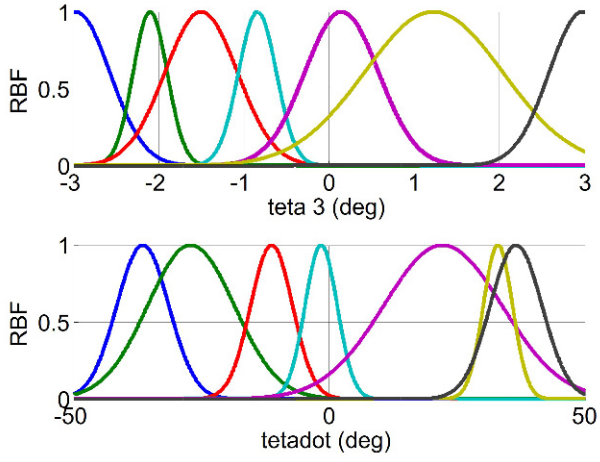

Fig. 6. Guassisn functions of torso NNs (position and velocity) at the end of off-line training phase.

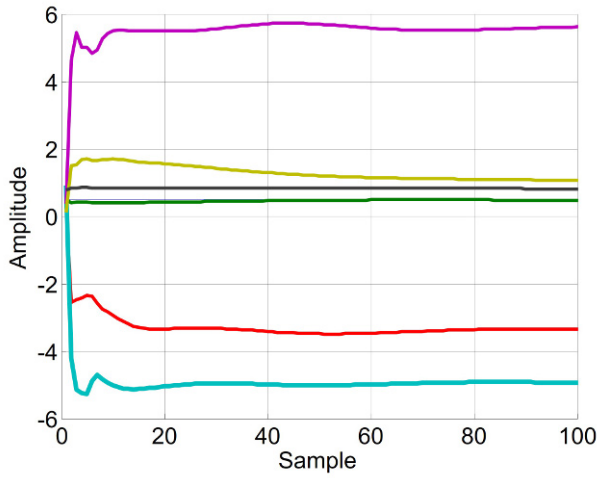

Fig. 7. Weights of torso NN for prediction of angular position at the end of off-line training phase.

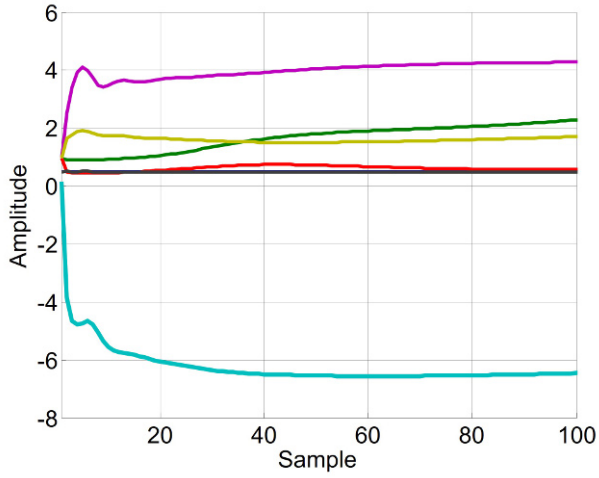

Fig. 8. Weights of torso NN for prediction of angular velocity at the end of off-line training phase.

Then, the free parameters of the RBFNN are updated according to the following equations [24]:

$$
\begin{aligned}
&w_j(k) = w_j(k-1) + \Delta w_j(k),\\
&b_j(k) = b_j(k-1) + \Delta b_j(k),\\
&c_{ji}(k) = c_{ji}(k-1) + \Delta c_{ji}(k)\\
&\Delta w_j(k) = -\eta \frac{\partial E}{\partial w_j} = \eta(y(k) - y_{\mathrm{RBF}}(k)), \qquad (19)\\
&\Delta b_j(k) = -\eta \frac{\partial E}{\partial b_j} = \eta(y(k) - y_{\mathrm{RBF}}(k)) w_j h_j \frac{\|\mathbf{x} - \mathbf{c}_j\|^2}{b_j^3},\\
&\Delta c_{ji}(k) = -\eta \frac{\partial E}{\partial c_{ji}} = \eta(y(t) - y_{\mathrm{RBF}}(k)) w_j \frac{x_j - c_{ji}}{b_j^2},
\end{aligned}
$$

where $\eta \in [0,1]$ is the learning rate. During the off-line training, all network parameters are trained. However, during the on-line training, in order to reduce the computation time, only the weights in the output layer are trained. The off-line training is performed using 400 input-output data that are gathered using the computed torque method. Fig. 6 shows the Gaussian functions and Figs. 7 and 8 show the weights of the output layer of NNs for the torso at the end of the off-line training phase.

5. STABILITY ANALYSIS

The stability of the biped locomotion can be analyzed using the Lyapunov direct method or Poincaré map. Since walking is a periodic motion, the Lyapunov stability method provides only stability in single step of the robot, whereas the Poincaré map shows stability of the robot in general. However, using the Poincaré map method for a highly nonlinear system such as the biped robots is not very straightforward. Both of these methods are presented in the sequel. The general equation of a biped robot with n

DOF can be expressed in the form of a nonlinear discrete-time system as

$$\mathbf{x}(k+1) = \mathbf{f}(\mathbf{x}(k), \mathbf{u}(k)), \tag{20}$$

where $\mathbf{x}(k) \in R^{n\times 1}$ and $\mathbf{u}(k) \in R^{n\times 1}$ are the control input and state vector of the system, respectively, $\mathbf{f}$ is a nonlinear discrete function that has an equilibrium point at the origin ($\mathbf{f}(\mathbf{0},\mathbf{0}) = \mathbf{0}$). The nonlinear optimization problem can be defined as the following cost function and the set of constraints for a biped robot:

$$\mathbf{u}^* = \arg\min_{\mathbf{U}}(C(k)) \tag{21}$$

such that

$$\begin{aligned} C(k) &= \sum_{j-1}^{N_p} Q\left(\frac{e^{D_{ZMP}(k+j|k)} - e^{D_{ZMP_{\min}}}}{e^{D_{ZMP_{\max}}} - e^{D_{ZMP_{\min}}}}\right) \\ &\quad + \sum_{j=1}^{N_c} \mathbf{u}^T(k+j|k)\mathbf{R}\mathbf{u}(k+j|k), \\ \mathbf{x}(k|k) &= \mathbf{x}(k) = \mathbf{x}_0, \\ y(k+j+1|k) &= \mathbf{h}(\mathbf{x}(k+j|k)), \\ \mathbf{x}_{\min} &\le \mathbf{x}(k+j|k) \le \mathbf{x}_{\max}, \\ \mathbf{u}_{\min} &\le \mathbf{u}(k+j|k) \le \mathbf{u}_{\max}, \end{aligned} \tag{22}$$

where $\mathbf{x} = [\theta_1, ..., \theta_n, \dot{\theta}_1, ..., \dot{\theta}_n]^T$ is the angular position and velocity vector and $\mathbf{u} = [u_1, ..., u_n]^T$ is the control input.

5.1. Lyapunov method

For a biped robot, the Lyapunov function can be defined as

$$\begin{aligned} V(\mathbf{x}(k)) &= \sum_{j=1}^{N_p} L(\mathbf{x}^*(k+j|k)) \\ &= \sum_{j=1}^{N_p} \left(\frac{e^{D_{ZMP}(k+j|k)} - e^{D_{ZMP_{\min}}}}{e^{D_{ZMP_{\max}}} - e^{D_{ZMP_{\min}}}}\right), \end{aligned} \tag{23}$$

where $\mathbf{x}^*$ is the optimal solution of the optimization problem in (22); other parameters were defined in (5). Due to the constraints on the states and inputs, it may not be possible to study the globally stability of the biped robot using the Lyapunov method. Hence, the stability region for the predictive control is defined as follows. Throughut this paper, the notation $a(m|n)$ indicates the value of a at instant m predicted at instant n.

Definition 1: The stability region for the predictive control problem is defined as a set in which for every $\mathbf{x}(k) \in \chi$ there exists a control signal $u(k) \in v$ such that [25]

$$\begin{cases} \mathbf{x}(k+1) \in \chi, \\ L(\mathbf{x}(k+2|k)) - L(\mathbf{x}(k+1|k)) \le 0. \end{cases} \tag{24}$$

Theorem 1: Consider the NMPC problem for the system (20) with the cost function (5). The closed-loop system is locally stable within the stability region and around the origin if

$$\begin{cases} \mathbf{x}^*(k|k) = \mathbf{x}(k) \in \chi \quad \forall k, \\ \mathbf{X}^*(k|k) = [\mathbf{x}^*(k+1|k), ..., \mathbf{x}^*(k+N_p|k)] \in \chi. \end{cases} \tag{25}$$

Proof: The first difference of $V(\mathbf{x}(k))$ in (23) is

$$\begin{aligned} \Delta V(\mathbf{x}(k)) &= V(\mathbf{x}(k)) - V(\mathbf{x}(k-1)) \\ &= \sum_{j=1}^{N_p} \{L(\mathbf{x}^*(k+j+1|k+1)) \\ &\qquad - L(\mathbf{x}^*(k+j|k))\}. \end{aligned} \tag{26}$$

After solving the optimization problem at time instant k, the obtained optimal control sequence over the prediction horizon is

$$\mathbf{U}^*(k|k) = [\mathbf{u}^*(k|k), ..., \mathbf{u}^*(k+N_p|k)]^T. \tag{27}$$

The first element of $\mathbf{U}^*(k|k)$ is applied to the system at time instant $k+1$; hence

$$\mathbf{x}(k+1) = \mathbf{x}^*(k+1|k). \tag{28}$$

The new control sequence at time instant $k+1$ will be

$$\begin{aligned} &\tilde{\mathbf{U}}(k+1|k+1) = [\tilde{\mathbf{u}}(k+1|k+1), ..., \tilde{\mathbf{u}}(k+N_p|k+1)]^T, \\ &\tilde{\mathbf{u}}(k+i|k+1) = \mathbf{u}^*(k+i|k); \quad i = 1, ..., N_p. \end{aligned} \tag{29}$$

The control sequence $\tilde{\mathbf{U}}(k+1|k+1)$ is not necessarily the optimal control sequence. The state vector corresponding to the control sequence $\tilde{\mathbf{U}}(k+1|k+1)$ with the initial state of the system $\mathbf{x}(k+1)$ is equal to

$$\begin{aligned} &\tilde{\mathbf{X}}(k+1|k+1) \\ &= [\tilde{\mathbf{x}}(k+2|k+1), ..., \tilde{\mathbf{x}}(k+N_p+1|k+1)]. \end{aligned} \tag{30}$$

The Lyapunov function corresponding to $\tilde{\mathbf{X}}(k+1|k+1)$ is defined as

$$\tilde{V}(\tilde{\mathbf{x}}(k+1)) = \sum_{j=1}^{N_p} L(\tilde{\mathbf{x}}(k+j+1|k+1)). \tag{31}$$

Therefore, $\tilde{V}(\tilde{\mathbf{x}}(k+1))$ is not necessarily optimal at time instant $k+1$ and one can conclude that

$$V(\mathbf{x}(k+1)) \le \tilde{V}(\tilde{\mathbf{x}}(k+1)). \tag{32}$$

Thus,

$$\Delta V(\mathbf{x}(k)) \le \tilde{V}(\tilde{\mathbf{x}}(k+1)) - V(\mathbf{x}(k)). \tag{33}$$

Moreover,

$$\begin{cases} \tilde{\mathbf{x}}(k+i|k+1) = \mathbf{x}^*(k+i|k); \quad i = 2, ..., N_p, \\ \tilde{\mathbf{x}}(k+N_p+1|k+1) = \mathbf{f}(\mathbf{x}^*(k+N_p|k), \mathbf{u}^*(k+N_p|k)). \end{cases} \tag{34}$$

Substituting (34) into (33) yields

$$\Delta V(\mathbf{x}(k)) \leq \sum_{j=1}^{N_p} L(\tilde{\mathbf{x}}(k+j+1|k+1)) - \sum_{j=1}^{N_p} L(\mathbf{x}^*(k+j|k)). \tag{35}$$

Therefore,

$$\begin{aligned}\Delta V(\mathbf{x}(k)) \leq & L(\tilde{\mathbf{x}}(k+N_p+1|k+1)) \\ & + \sum_{j=1}^{N_p-1} L(\tilde{\mathbf{x}}(k+j+1|k+1)) \\ & - \sum_{j=2}^{N_p} L(\mathbf{x}^*(k+j|k) - L(\mathbf{x}^*(k+1|k))).\end{aligned} \tag{36}$$

Using (29) and (34), (36) can be written as

$$\Delta V(\mathbf{x}(k)) \leq L(\tilde{\mathbf{x}}(k+N_p+1|k+1)) - L(\mathbf{x}^*(k+1|k)). \tag{37}$$

Hence,

$$\Delta V(\mathbf{x}(k)) \leq L(\mathbf{f}(\mathbf{x}^*(k+N_p|k))) - L(\mathbf{x}^*(k+1|k)). \tag{38}$$

Equation (38) can be written in a simple form as

$$\Delta V(\mathbf{x}(k)) \leq L_{N_p} - L_0, \tag{39}$$

where L_0 and L_{N_p} are the value of the nonlinear function $L(\cdot)$ at the beginning and end of the optimization process over the prediction horizon. According to Definition 1, inequality $L_{N_p} < L_0$ is satisfied for a predictive control. Therefore,

$$\Delta V(\mathbf{x}(k)) \leq 0. \tag{40}$$

Thus, $\Delta V(\mathbf{x}(k))$ is negative within the region χ and based on the Lyapunov stability theory, the closed-loop system is locally stable. □

5.1.1 Poincaré map method

In this section, the globally stability analysis of the biped locomotion is analyzed using the Poincaré map. This method can be used for stability analysis of the continuous dynamical systems that exhibits periodic or quasi-periodic behavior. The Poincaré map is the return of one point on the Poincaré section to the next point on this section. For a continuous dynamical system, the Poincaré map is the intersection of the periodic orbit in the state space with Poincaré section [26]. In this way, the stability study of the periodic orbit of a continuous dynamical system reduces to a discrete dynamical system with lower-dimensional state space, which has equilibrium points. This discrete system has the same stability property as the original system.

5.1.2 Poincaré map for biped robot

For a walking robot, a natural selection of the Poincaré section can be the walking surface (i.e., the ground), where the impact takes place. Hence, the Poincaré map for a biped robot is the intersection of the walking surface with the periodic orbit of the state variables. The stability of this orbit was studied in the previous section using the Lyapunov method. However, the biped robots are hybrid dynamical systems with SSP, impact, and DSP. In the DSP, both leg of the biped robot have contact with the ground and the robot is more stable. Therefore, one can study only the stability of the biped robot in the SSP and impact phase [19, 21]. Systems with impulse effects can be used to study the biped locomotion. These systems have a continuous phase that are described by a differential equation, and a discrete phase. To define a control system with impulse effects, consider a nonlinear control system represented as

$$\dot{\mathbf{x}} = \mathbf{f}(\mathbf{x}) + \mathbf{g}(\mathbf{x})\mathbf{u}, \tag{41}$$

where $\mathbf{x}$ and $\mathbf{u}$ are the state and control input vectors, respectively, and $\mathbf{f}(\cdot)$ and $\mathbf{g}(\cdot)$ are known and nonlinear functions. A control system with impulse effects has the following form:

$$\Sigma : \begin{cases} \dot{\mathbf{x}} = \mathbf{f}(\mathbf{x}) + \mathbf{g}(\mathbf{x})\mathbf{u}, & \mathbf{x}^- \notin S, \\ \mathbf{x}^+ = \Delta(\mathbf{x}^-), & \mathbf{x}^- \in S, \end{cases} \tag{42}$$

where S is the impact surface and $\mathbf{x}^-$ and $\mathbf{x}^+$ are the state vector right before and after the impact, respectively. To obtain the state space form for the biped robot, the system state vector is defined as

$$\mathbf{x} = \left[\boldsymbol{\theta}^T, \dot{\boldsymbol{\theta}}^T\right]^T, \tag{43}$$

where $\boldsymbol{\theta}$ and $\dot{\boldsymbol{\theta}}$ are the angular position and velocity of the joints, respectively. The dynamic equation for the biped robot in the SSP is expressed as

$$\mathbf{D}(\boldsymbol{\theta})\ddot{\boldsymbol{\theta}} + \mathbf{H}(\boldsymbol{\theta}, \dot{\boldsymbol{\theta}})\dot{\boldsymbol{\theta}} + \mathbf{G}(\boldsymbol{\theta}) = \boldsymbol{\tau}. \tag{44}$$

The state-space form of the differential equation (44) can be written as follows:

$$\dot{\mathbf{x}} = \begin{bmatrix} \dot{\boldsymbol{\theta}} \\ \mathbf{D}^{-1}(\boldsymbol{\theta})\left(-\mathbf{H}(\boldsymbol{\theta}, \dot{\boldsymbol{\theta}})\dot{\boldsymbol{\theta}} - \mathbf{G}(\boldsymbol{\theta})\right) \end{bmatrix} + \begin{bmatrix} \mathbf{0} \\ \mathbf{D}^{-1}(\boldsymbol{\theta}) \end{bmatrix} \boldsymbol{\tau}. \tag{45}$$

In order to present the dynamic equation of the biped robot to form a system with impulse effects, the functions $\mathbf{f}$ and $\mathbf{g}$ should be written in the following form:

$$\begin{aligned} \mathbf{f}(\mathbf{x}) &= \begin{bmatrix} \ddot{\boldsymbol{\theta}} \\ \mathbf{D}^{-1}(\boldsymbol{\theta})\left(-\mathbf{H}(\boldsymbol{\theta}, \dot{\boldsymbol{\theta}})\dot{\boldsymbol{\theta}} - \mathbf{G}(\boldsymbol{\theta})\right) \end{bmatrix}, \\ \mathbf{g}(\mathbf{x}) &= \begin{bmatrix} \mathbf{0} \\ \mathbf{D}^{-1}(\boldsymbol{\theta}) \end{bmatrix}. \end{aligned} \tag{46}$$

Moreover, the impact map can be written as

$$\dot{\boldsymbol{\theta}}^{+} = \dot{\boldsymbol{\theta}}^{-} + \mathbf{D}^{-1}(\boldsymbol{\theta})\mathbf{J}(\boldsymbol{\theta}) \left[\begin{array}{ccc} \mathbf{J}(\boldsymbol{\theta}) & \mathbf{D}^{-1}(\boldsymbol{\theta}) & \mathbf{J}^{T}(\boldsymbol{\theta}) \end{array} \right]^{-1} (-\mathbf{J}\dot{\boldsymbol{\theta}}^{-}). \tag{47}$$

In the impact phase, it is assumed that only the angular velocity of the joints change. Therefore, the state vector after the impact can be written as

$$\mathbf{x}^{+} = \Delta(\mathbf{x}^{-}) = \left[\begin{array}{c} \Delta(\boldsymbol{\theta}^{-}) \\ \Delta(\boldsymbol{\theta}^{-}, \dot{\boldsymbol{\theta}}^{-}) \end{array} \right] = \left[\begin{array}{c} \mathbf{1} \\ \Delta(\boldsymbol{\theta}^{-}, \dot{\boldsymbol{\theta}}^{-}) \end{array} \right], \tag{48}$$

where

$$\Delta(\boldsymbol{\theta}^{-}, \dot{\boldsymbol{\theta}}^{-}) = \dot{\boldsymbol{\theta}}^{-} + \mathbf{D}^{-1}(\boldsymbol{\theta})\mathbf{J}^{T}(\boldsymbol{\theta}) \left[\begin{array}{ccc} \mathbf{J}(\boldsymbol{\theta}) & \mathbf{D}^{-1}(\boldsymbol{\theta}) & \mathbf{J}^{T}(\boldsymbol{\theta}) \end{array} \right]^{-1} (-\mathbf{J}\dot{\boldsymbol{\theta}}^{-}). \tag{49}$$

The impact surface can be defined as

$$S = \{\mathbf{x} \mid y_e(\boldsymbol{\theta}) = 0,\ x_e(\boldsymbol{\theta}) > x_b\}, \tag{50}$$

where $[x_e(\boldsymbol{\theta}), y_e(\boldsymbol{\theta})]^T$ is the coordinate of the tip of the swing leg and x_b is the horizontal position of the stance leg. Each step of the biped locomotion consists of an SSP and leg-support-exchange event. First, the Poincaré map is calculated for each phase. Then, the Poincaré map for a complete step can be obtained by combining them.

By defining $\mathbf{z} = [\boldsymbol{\theta}^T, \dot{\boldsymbol{\theta}}^T]^T$. (44) can be written as a first order system as

$$\dot{\mathbf{z}} = \left[\begin{array}{c} \dot{\boldsymbol{\theta}} \\ \mathbf{D}^{-1}(\boldsymbol{\theta}) \left(\boldsymbol{\tau} - \mathbf{H}(\boldsymbol{\theta}, \dot{\boldsymbol{\theta}})\dot{\boldsymbol{\theta}} - \mathbf{G}(\boldsymbol{\theta}) \right) \end{array} \right] = \mathbf{f}(\mathbf{z}), \tag{51}$$

where $\mathbf{z}_0 = \mathbf{z}(0) = \left[\boldsymbol{\theta}^T(0), \dot{\boldsymbol{\theta}}^T(0)\right]^T$ is the initial condition of the system. Then, the Poincaré map $\mathbf{P}_1$ for the SSP is as follows [22]:

$$\mathbf{P}_1 = \left[\begin{array}{c} \boldsymbol{\theta}^{-} \\ \dot{\boldsymbol{\theta}}^{-} \end{array} \right] = \int \left[\begin{array}{c} \dot{\boldsymbol{\theta}} \\ \mathbf{D}^{-1}(\boldsymbol{\theta}) \left(\boldsymbol{\tau} - \mathbf{H}(\boldsymbol{\theta}, \dot{\boldsymbol{\theta}})\dot{\boldsymbol{\theta}} - \mathbf{G}(\boldsymbol{\theta}) \right) \end{array} \right], \tag{52}$$

where $[\boldsymbol{\theta}^{-}, \dot{\boldsymbol{\theta}}^{-}]^T$ is a 10×1 vector that represents the angular position and velocity of the joints right before the impact, respectively. The integral in (52) can be solved by any suitable numerical method.

When the tip of the swing leg touches the ground, the impact occurs and only the angular velocities change. Therefore, the angular positions and velocities right after the impact can be written as

$$\left[\begin{array}{c} \boldsymbol{\theta}^{+} \\ \dot{\boldsymbol{\theta}}^{+} \end{array} \right] = \left[\begin{array}{c} \boldsymbol{\theta}^{-} \\ \dot{\boldsymbol{\theta}}^{-} + \mathbf{D}^{-1}(\boldsymbol{\theta})\mathbf{J}^{T}(\boldsymbol{\theta}) \left[\mathbf{J}(\boldsymbol{\theta})\ \mathbf{D}^{-1}(\boldsymbol{\theta})\ \mathbf{J}^{T}(\boldsymbol{\theta}) \right]^{-1} (-\mathbf{J}\dot{\boldsymbol{\theta}}^{-}) \end{array} \right]. \tag{53}$$

After the impact, the roles of the swing and stance legs exchange. Then, by relabeling the links, the same set of equations of motion can be used for both left and right legs. The positions and velocities of the joints at the end of each step are used as the initial conditions for the next step. The following matrix performs this transformation:

$$\mathbf{R} = \left[\begin{array}{cccccccccc} 0 & 0 & 0 & 0 & -1 & 0 & 0 & 0 & 0 & 0 \\ 0 & 0 & 0 & -1 & 0 & 0 & 0 & 0 & 0 & 0 \\ 0 & 0 & 1 & 0 & 0 & 0 & 0 & 0 & 0 & 0 \\ 0 & -1 & 0 & 0 & 0 & 0 & 0 & 0 & 0 & 0 \\ -1 & 0 & 0 & 0 & 0 & 0 & 0 & 0 & 0 & 0 \\ 0 & 0 & 0 & 0 & 0 & 0 & 0 & 0 & 0 & -1 \\ 0 & 0 & 0 & 0 & 0 & 0 & 0 & 0 & -1 & 0 \\ 0 & 0 & 0 & 0 & 0 & 0 & 0 & 1 & 0 & 0 \\ 0 & 0 & 0 & 0 & 0 & 0 & -1 & 0 & 0 & 0 \\ 0 & 0 & 0 & 0 & 0 & -1 & 0 & 0 & 0 & 0 \end{array} \right]. \tag{54}$$

Therefore, the second part of the Poincaré map ($\mathbf{P}_2$) can be expressed as

$$\mathbf{P}_2 = \mathbf{R} \left[\begin{array}{c} \boldsymbol{\theta}^{+} \\ \dot{\boldsymbol{\theta}}^{+} \end{array} \right] = \mathbf{R} \left[\begin{array}{c} \boldsymbol{\theta}^{-} \\ \dot{\boldsymbol{\theta}}^{-} + \mathbf{D}^{-1}(\boldsymbol{\theta})\mathbf{J}^{T}(\boldsymbol{\theta}) \left[\mathbf{J}(\boldsymbol{\theta})\ \mathbf{D}^{-1}(\boldsymbol{\theta})\ \mathbf{J}^{T}(\boldsymbol{\theta}) \right]^{-1} (-\mathbf{J}\dot{\boldsymbol{\theta}}^{-}) \end{array} \right]. \tag{55}$$

Combining $\mathbf{P}_1$ and $\mathbf{P}_2$, the Poincaré map (P) for a complete step of the biped locomotion can be expressed as [22]

$$\mathbf{P} = \mathbf{R} \left[\begin{array}{c} \boldsymbol{\theta}^{-} \\ \dot{\boldsymbol{\theta}}^{-} + \mathbf{D}^{-1}(\boldsymbol{\theta})\mathbf{J}^{T}(\boldsymbol{\theta}) \left[\mathbf{J}(\boldsymbol{\theta})\ \mathbf{D}^{-1}(\boldsymbol{\theta})\ \mathbf{J}^{T}(\boldsymbol{\theta}) \right]^{-1} (-\mathbf{J}\dot{\boldsymbol{\theta}}^{-}) \end{array} \right]. \tag{56}$$

In order to examine the stability of the biped locomotion, the fixed point of the Poincaré map in (56) should be inspected. This fixed point can be calculated using numerical integration methods. One way to determine the stability of this fixed point is to find the eigenvalues of the linearized Poincaré map. In other words, in order to have a stable system, all the eigenvalues of the linearized Poincaré map, evaluated around the fixed point, should be inside the unit circle.

However, in the proposed method, there is no predefined path for the biped robot to find the fixed point of the Poincaré map. This is because the walking pattern of the robot using the proposed method can be considered as quasi-periodic [27]. In other words, the impact does not

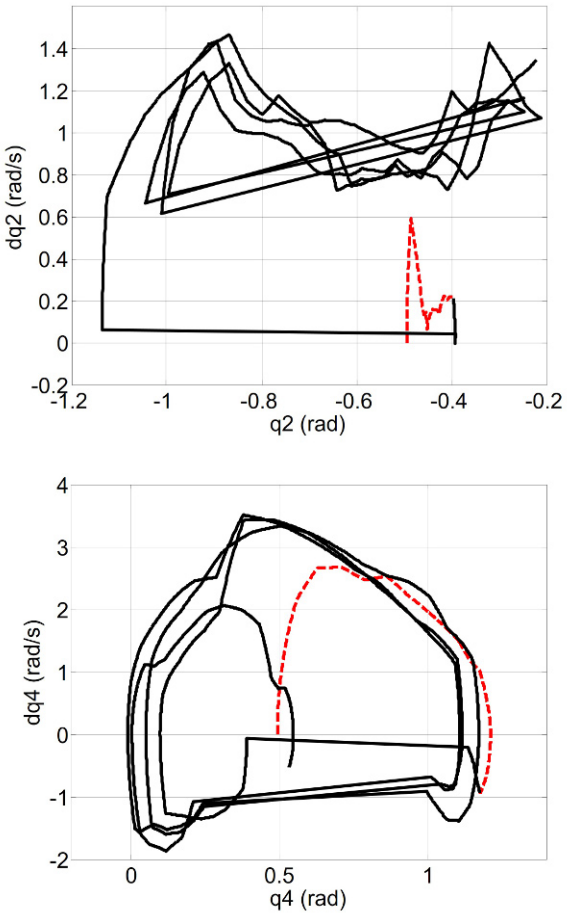

Fig. 9. Phase plane of the second and fourth joints.

happen at the exact same point ($\mathbf{x}^+$) on the impact surface (S) during walking of the robot. Fig. 9 shows the phase plane for the second and fourth (i.e., the knee) joints of the robot when ascending the stairs. This is a directed graph and each cycle indicates one complete gait of the robot. The red-dashed lines indicate the transition from the initial state to the periodic movement of the robot. The rest of the walking patterns are similar but not the same. That is why it is considered as quasi-periodic orbits. This is due to the nature of the proposed method, which adaptively defines the gait of the robot based on the constraints of the robot as well as the environment. In this way, the robot walks more naturally and closer to the humans walking.

To evaluate the fixed point of the Poincaré map, we have to find an average of several repetitions of walking. For this reason, the robot has walked up and down the stairs for fifty times with different initial conditions. The states of the robot are recorded right before the impact occurs. The Poincaré fixed point is the average of these recorded data. The fixed point $\mathbf{x}^* = [\boldsymbol{\theta}^{*-}, \dot{\boldsymbol{\theta}}^{*-}]$, for ascending and descending the stairs are as follows:

for ascending the stairs:

$$\boldsymbol{\theta}^{*-} = [0.4900, -0.2740, 0.0290, 1.0470, -0.3731]^T, \tag{57}$$

$$\dot{\boldsymbol{\theta}}^{*-} = [-0.0138, 0.8431, 0.1523, -0.6550, -0.1283]^T, \tag{58}$$

for descending the stairs:

$$\boldsymbol{\theta}^{*-} = [1.0048, -0.2834, 0.0173, 0.4351, -0.3098]^T, \tag{59}$$

$$\dot{\boldsymbol{\theta}}^{*-} = [0.1011, 1.2504, 0.1130, -1.3333, 0.0504]^T. \tag{60}$$

Next, the Poincaré map P is linearized around the fixed point $\mathbf{x}^* = [\boldsymbol{\theta}^{*-}, \dot{\boldsymbol{\theta}}^{*-}]$

$$\delta \mathbf{x}^{k+1} = \mathbf{A} \delta \mathbf{x}^k, \tag{61}$$

where the 10×10 matrix $\mathbf{A}$ is the Jacobian of the Poincaré map and is computed as follows [21]:

$$\begin{aligned} &\mathbf{A} = \begin{bmatrix} \mathbf{A}_1 & \mathbf{A}_2 & \dots & \mathbf{A}_n \end{bmatrix}, \\ &\mathbf{A}_j = \frac{\mathbf{P}(\mathbf{x}^* + \Delta \mathbf{x}_i) - \mathbf{P}(\mathbf{x}^* - \Delta \mathbf{x}_i)}{2\Delta \mathbf{x}_i}, \quad i = 1, \dots, 10, \end{aligned} \tag{62}$$

where the ith element of $\Delta \mathbf{x}_i$ is defined as

$$\begin{cases} \Delta x_i = \Delta \theta_i, & i = 1, \dots, 5, \\ \Delta x_i = \Delta \dot{\theta}_i, & i = 6, \dots, 10. \end{cases} \tag{63}$$

Considering $\Delta x_i = 0.05$, matrix $\mathbf{A}$ can be computed. The eigenvalues of the Jacobian matrix $\mathbf{A}$ for ascending the stairs are

$$\begin{aligned} &\lambda_1 = -0.7254, \quad \lambda_2 = -0.5464, \\ &\lambda_{3,4} = -0.0264 \pm j\, 0.0804, \\ &\lambda_{5,6} = 0.4710 \pm j\, 0.3619, \\ &\lambda_7 = 0.9353, \quad \lambda_{8,9} = 0.7099 \pm j\, 0.0562, \\ &\lambda_{10} = 0.5956, \end{aligned} \tag{64}$$

and for descending the stairs they are equal to

$$\begin{aligned} &\lambda_{1,2} = -0.6319 \pm j\, 0.2820, \\ &\lambda_{3,4} = -0.0112 \pm j\, 0.0756, \\ &\lambda_{5,6} = 0.6549 \pm j\, 0.3766, \quad \lambda_7 = 0.7273, \\ &\lambda_{8,9} = 0.6032 \pm j\, 0.0735, \quad \lambda_{10} = 0.5540, \end{aligned} \tag{65}$$

which show that all eigenvalues of $\mathbf{A}$ for the discontinuous Poincaré map are inside the unit circle for walking up and down the stairs. Hence, the closed-loop system is globally stable.

6. SIMULATION RESULTS

This section presents simulation results on the biped robot in ascending and descending the stairs. For model prediction, the RBFNNs (Section 3) are employed. The physical parameters of the robot are given in Table 1. Table 2 shows the minimum and maximum of the constraints. Other parameters are as follows:

$$\text{Foot Length} = 0.2 \text{ m}, \ N_p = 5, \ N_c = 4, \ Q = 100, \ \mathbf{R} = 0.01\mathbf{I}, \ \Delta t = 30 \text{ ms}, \ \delta = 1.5, \ ZMP_{\min} = x_b, \ ZMP_{\max} = x_b + 0.2.$$

The value of Q and $\mathbf{R}$ are selected in order for both terms in (5) to have almost the same effect on the cost function. Other parameters (β, δ, N_p, and N_c) are selected for the best performance of the proposed method.

The nonlinear constraint optimization problem in the NMPC is solved using the fmincon function in the MATLAB optimization toolbox. This function is based on the Sequential Quadratic Programming (SQP). The SQP is an iterative technique in which the objective is replaced by a quadratic approximation and the constraints by linear approximations [28].

In the first part of simulations, the height and depth of all stairs are the same and equal to 0.35 m and 0.2 m, respectively. Moreover, the dynamic differential equation of the biped robot is used as the predictor model in the NMPC. The simulation results are shown in Figs. 10 to 13. Fig. 10 shows the stick diagram of the biped robot in ascending and descending the stairs and walking on a flat surface. Fig. 11 shows that the horizontal position of the ZMP moves forward and is within the support polygon at all times in the SSP as well as in the DSP. Therefore, the biped robot is dynamically balanced. The vertical and horizontal position of the swing and stance legs are shown in Figs. 12 and 13, respectively.

Most papers on the subject of this manuscript assume a fixed height and depth for all strairs, which is not the case in reality. Even if they are fixed, their value should be measured a priori and given to the control algorithm before the robot can walk. On the other hand, in this paper, there are no predefined gait for the proposed control method. This means that the robot can climb stairs with different heights and depths. In other words, using the proposed method, the robot does not need to known the trajectory in advance and just real-time information from the stairs that are obtained from the sensors (e.g., cameras) suffices to control the robot in ascending and descending random stairs. This situation can aslo be considered as walking on rough terrains.

Fig. 14 shows the flexibility of the proposed method for the on-line trajectory generation in climbing the stairs with defferent heights and depths. Figs. 15, 16 and 17 show the horizontal position of the ZMP and the horizontal and vertical position of the right and left legs, respectively, which

Table 1. Physical parameters of 5-DOF biped.

Link	Length (m)	Mass (kg)	Inertia (kgm^2)	Location of COM (m)
1, 5	0.54	3.7	0.5	0.285
2, 4	0.5	8.55	0.5	0.31
3	0.7	25	0.5	0.4

Table 2. Minimum and maximum values of variables.

Variable	Minimum	Maximum
θ_1	0°	30°
θ_2	−60°	0°
θ_3	−3°	3°
θ_4	0°	80°
θ_5	−80°	0°
T_i	−350Nm	350Nm
β	4	15

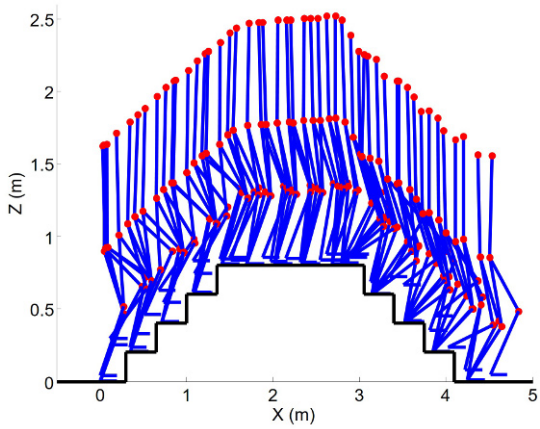

Fig. 10. Stick diagram of biped robot in ascending and descending the stairs.

show the success of the proposed method in climbing random stairs. Fig. 18 shows that the joint torques are within the saturation limits (±350 Nm). Fig. 19 shows the horizontal velocity of the COM. As this figure shows, during the fourth step (i.e., when the stair height is high), the controller decreases the velocity of the robot in order to maintain the stability. The dynamic walking of the robot can be observed from this figure. It should be mentioned that the velocity of the robot is not predefined and the controller determines it based on the physical constraints of the robot. In this way, walking of the robot is more natural and closer to the human walking.

Next, the performance of the NMPC is investigated in the presence of robots uncertainties and external disturbances. In this case, the RBFNN is employed for model prediction. For robots uncertainty, a 30% increase in the mass and inertia of the torso link is considered. For exter-

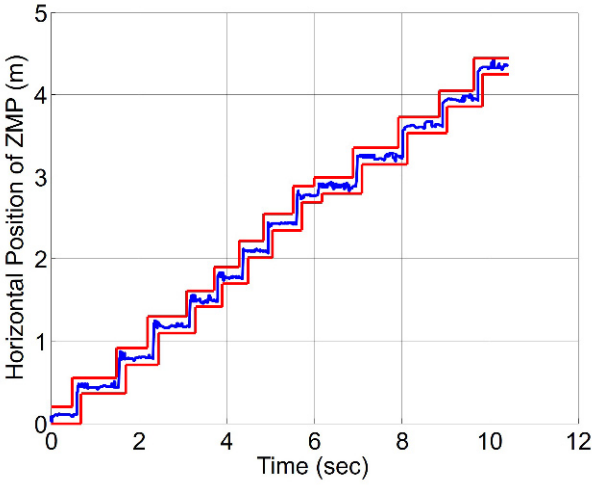

Fig. 11. Horizontal position of ZMP.

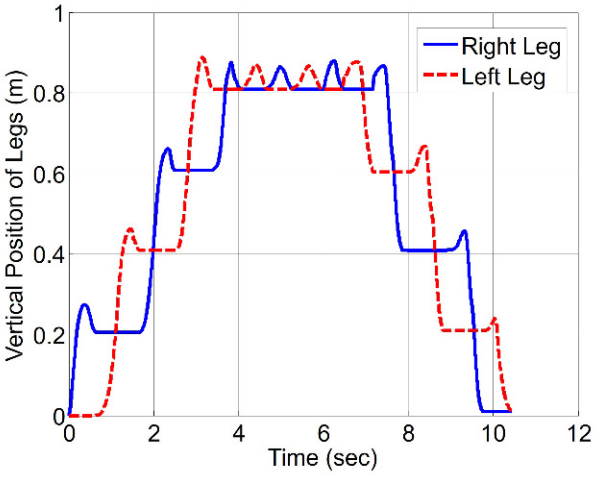

Fig. 12. Vertical position of the right and left legs.

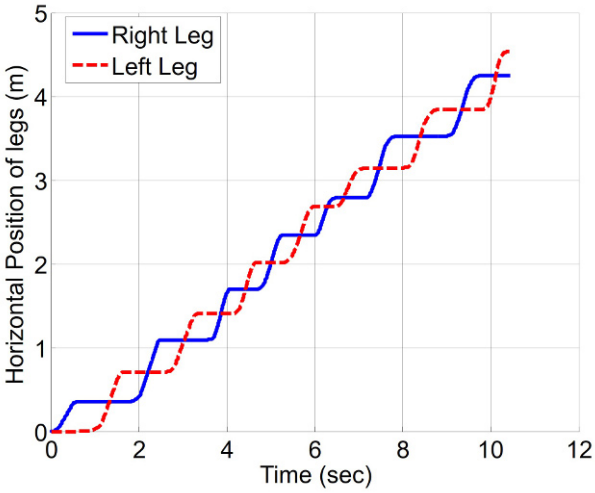

Fig. 13. Horizontal position of the right and left legs.

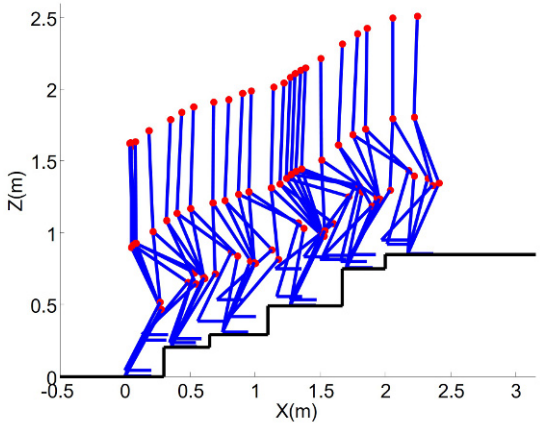

Fig. 14. Stable climbing stairs with different heights and depths.

nal disturbance, a 100 Nm impact torque is applied to the torso for 0.15 sec.

In order to show the vital role of the NNs, first the dynamic equations of the robot are used as the prediction model. As Figs. 20 and 21 show, the biped robot is not able to keep its stability and eventually falls down. To solve this problem, the RBFNN is used as the prediction model in the NMPC. In this case, the prediction model is able to adapt itself to the changes in the robot as well as in the environment (Fig. 22). Fig. 23 shows the horizontal position of the ZMP in the presence of uncertainty in the model of the robot. As this figure shows, the ZMP remains in the stable area. The horizontal position of the ZMP and the joint torques, when the external disturbance is exerted on the robot, are shown in Figs. 25 and 26, respectively.

In [5], for generating a stable trajectory, the desired ZMP is considered in the middle of the stance leg. Then, according to the relationship between the position of the COM and the ZMP, the trajectory of the COM in the horizontal direction is obtained by solving a second order differential equation. Moreover, by adjusting the length of the inverted pendulum, the ZMP error is reduced. In their method, the duration and length of each gait are fixed. Therefore, the biped robot is not able to climb the stairs with different height and depth. Hence, if the environment or the length and depth of the stairs change, the biped robot is not able to adapt itself to the new environment. In addition, the robot moves very slowly such that it can be considered as a static motion.

7. CONCLUSION

This paper proposed a nonlinear model predictive control scheme for a five-DOF biped robot for dynamic walking up and down the stairs. The main advantage of the

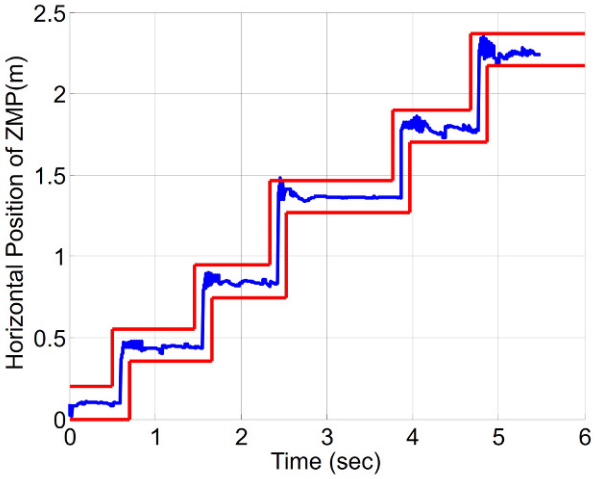

Fig. 15. Horizontal position of ZMP in climbing stairs with different heights and depths.

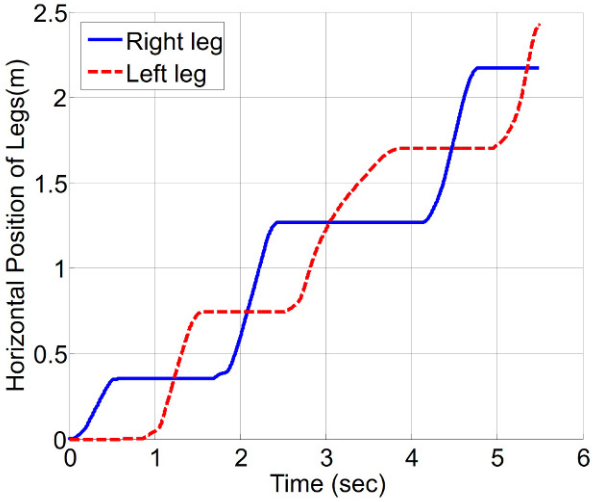

Fig. 16. Horizontal position of right and left legs in climbing stairs with different heights and depths.

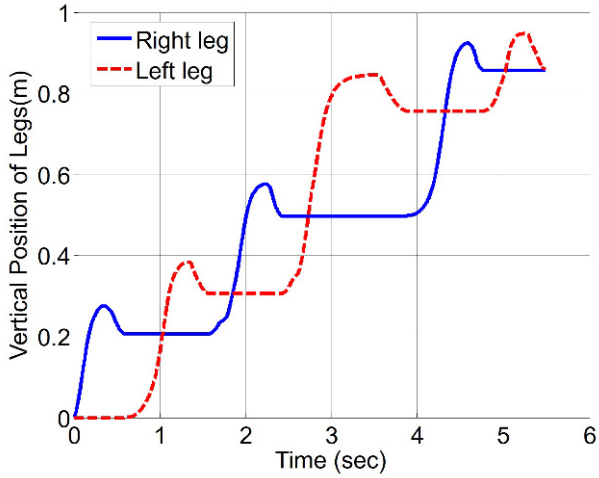

Fig. 17. Vertical position of right and left legs in climbing stairs with different heights and depths.

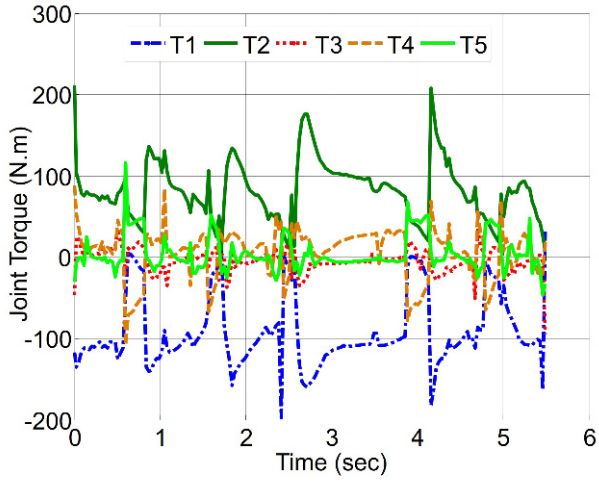

Fig. 18. Joint torques in climbing stairs with different heights and depths.

proposed method is that it does not require any predefined trajectory and the motion of the robot is expressed in the form of a cost function and some constraints for ascending and descending the stairs. Therefore, the trajectory generation is performed online. In other words, the motion of the biped robot can mimic the natural humans walking. Another advantage of the proposed method is that the length step is not fixed and the controller specifies it as robot involves in walking. Therefore, the robot can walk over stairs with different heights and depths. It was shown that the NMPC is a model-based scheme and to improve the performance of the controller, an accurate model of the robot is required. To this end, the RBFNN was used to model the robot dynamics accurately and the performance of the neuro-NMPC controller in the presence of the robots uncertainties and external disturbances was examined. The stability analysis of the closed-loop system was studied using the Lyapunov method and the Poincaré map. Simulating examples showed good performance of the proposed controller for climbing random stairs and coping with uncertainties in the system and external disturbances as well.

REFERENCES

[1] Q. Huang, K. Yokoi, S. Kajita, and K. Kaneko, "Planning walking patterns for a biped robot," *IEEE Transactions on Robotics and Automation*, vol. 17, no. 3, pp. 280-289, 2001.

[2] S. Kajita, F. Kanehiro, K. Kaneko, and K. Fujiwara, "Biped walking pattern generation by using preview control of

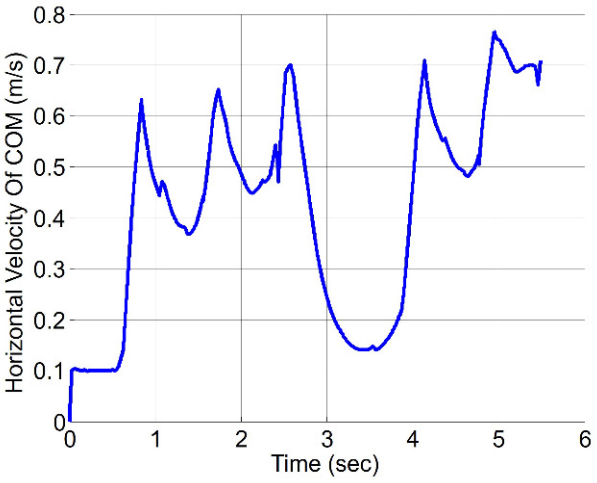

Fig. 19. Horizontal velocity of COM in climbing stairs with different heights and depths.

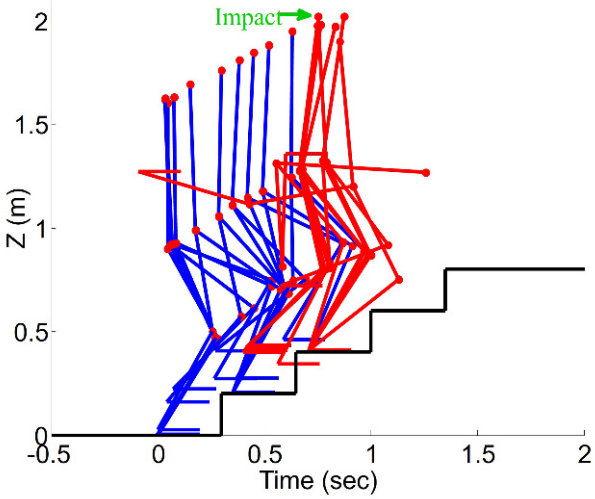

Fig. 21. Unstable biped robot in presence of external disturbance.

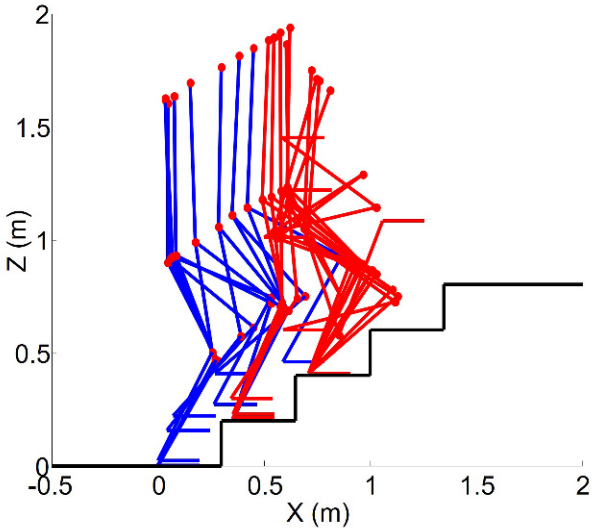

Fig. 20. Unstable biped robot in presence of uncertainty.

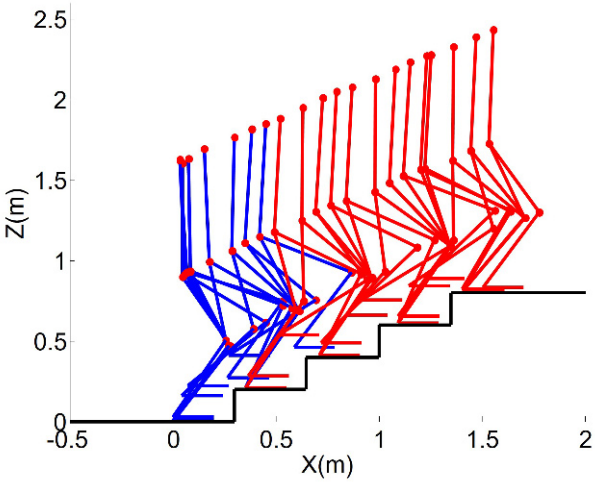

Fig. 22. Successful climbing in presence of uncertainty using RBFNN.

zero-moment point," *Proc. of IEEE International Conference on Robotics and Automation*, Taipai, Taiwan, Sept 2003.

[3] C. Zhou and Q. Meng, "Dynamic balance of a biped robot using fuzzy reinforcement learning agents," *Journal of Fuzzy Sets and Systems*, vol. 134, no. 1, pp. 169-187, 2003. [click]

[4] J. Y. Kim, I. W. park, and J. H. Oh, "Realization of dynamic stair climbing for biped humanoid robot using force/torque sensors," *Journal of Intelligent and Robotic Systems*, vol. 56, no. 4, pp. 389-423, 2009. [click]

[5] C. S. Park, T. ha, J. Kim, and C. H. Choi, "Trajectory generation and control for a biped robot walking upstairs," *International Journal of Control, Automation, and Systems*, vol. 8, no. 2, pp. 339-351, 2010. [click]

[6] O. Kwona and K. S. Jeon, "Optimal trajectory generation for biped robots walking up-and-down stairs," *Journal of Mechanical Science and Technology (KSME Int. J.)*, vol. 20, no. 5, pp. 612-620, 2-006.

[7] S. Ito, S. Amano, M. Sasaki, and P. Kulvanit, "A ZMP feedback control for biped balance and its application to in-place lateral stepping motion," *Journal of Computer*, vol. 3, no. 8, pp. 23-31, 2008.

[8] P. Sardain and G. Bessonnet, "Force acting on a biped robot. center of pressure-zero moment point," *IEEE Transactions on Systems, Man, and Cybernetics- Part A: Systems and Humans*, vol. 8, no. 5, pp. 1061-1071, 2010.

[9] M. Vukobratovic and D. Juricic, "Contribution to the synthesis of biped gait," *IEEE Transactions on Bio-Medical Engineering*, vol. 16, no. 1, pp. 1-6, 1969.

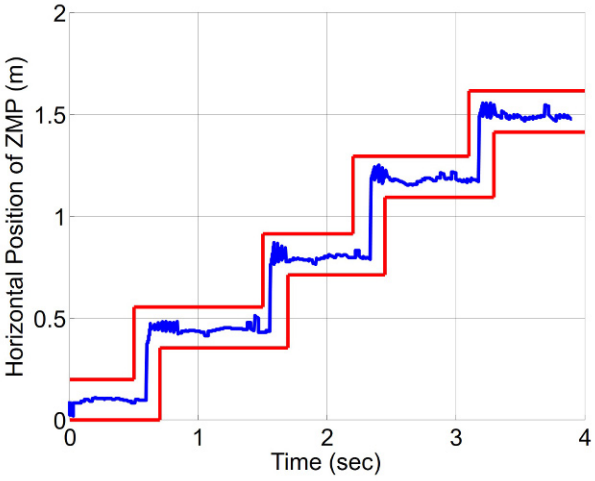

Fig. 23. ZMP in presence of uncertainty using RBFNN.

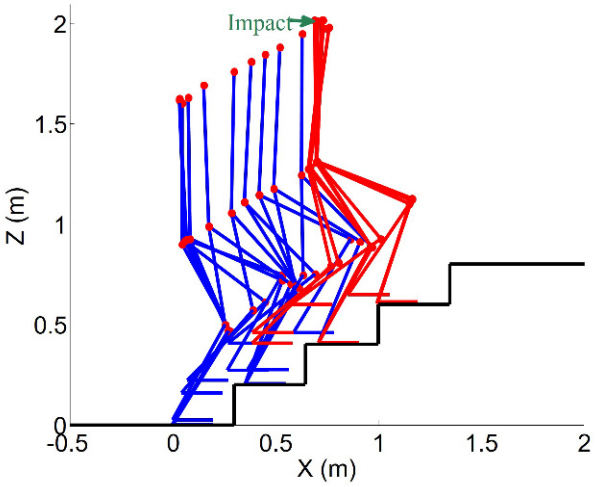

Fig. 24. Successful climbing in presence of external disturbace using RBFNN.

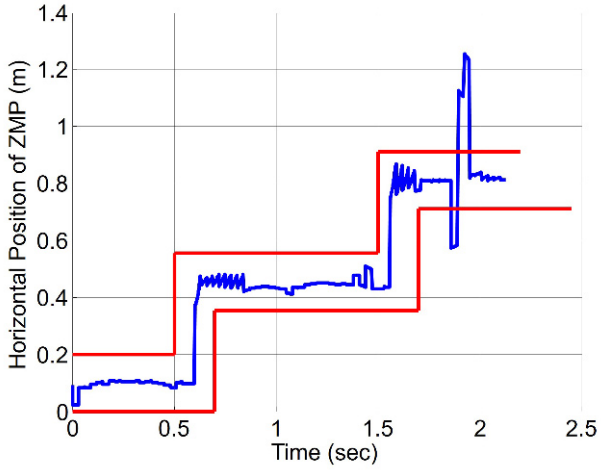

Fig. 25. ZMP in presence of external disturbace using RBFNN.

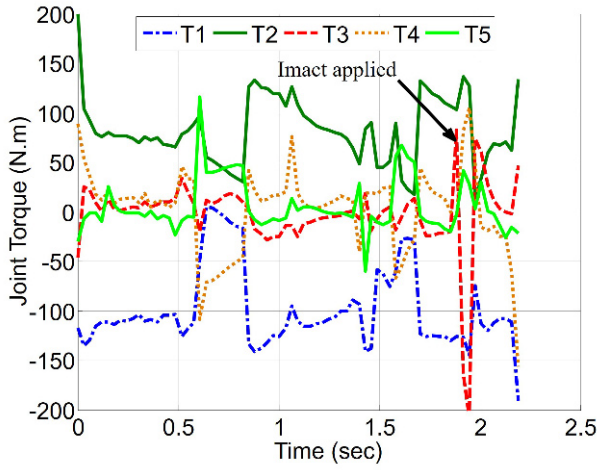

Fig. 26. Joint torques in presence of external disturbance using RBFNN.

[10] C. Fu and K. Chen, "Gait synthesis and sensory control of stair climbing for a humanoid robot," *IEEE Transactions on Electronics*, vol. 55, no. 5, pp. 2111-2120, 2008.

[11] Z. Zho, Y. Wang, and X. Chen, " Real-time control of full actuated biped robot based on nonlinear model predictive control," *International Conference on Intelligent Robotics*, vol. 5314, pp. 873-882, Wuhan, China, 2008. [click]

[12] H. Diedam, D. Dimitrov, P. B. Wieber, K. Mombaur, and M. Diehl, "Online walking gait generation with adaptive foot positioning through model predictive control," *Proc. of IEEE International Conference of Intelligent Robots and Systems*, Nice, France, 2008.

[13] D. Dimitrov, H. J. Ferreau, P. B. Wieber, M. Diehl, and I. Rhone-Alpes, "On the implementation of model predictive control for on-line walking pattern generation," *Proc. of IEEE International Conference on Robotics and Automation*, Pasadena, CA, USA, May 19-23, 2008.

[14] M. Parsa and M. Farrokhi, "Robust trajectory free model predictive control of biped robots with adaptive gait length," *International Journal of Robotics*, vol. 2, no. 1, pp. 46-55, 2011.

[15] P. B. Wieber, "Trajectory free linear model predictive control for stable walking in the presence of strong pertubations," *Proc. of International Coneference of Humanoid Robots*, Prague, 2006.

[16] M. Vukobratovic, A. A. Frank, and D. Juricic, "On stability of biped locomotion," *IEEE Transactions on Bio-Medical Engineering*, vol. 19, no. 1, pp. 25-36, 1970.

[17] F. Gubina, H. Hemami, and R. B. McGhee, "On the dynamic of biped locomotion," *IEEE Transactions on Bio-Medical Engineering*, vol. 21, no. 2, pp. 102-108, 1974.

[18] H. Hemami and B. Cheng, "Stability analysis and input design of a two-link planar biped," *International Journal Robotics Research*, vol. 3, no. 2, pp. 93-100, 1984.

[19] J. W. Grizzle, G. Abba, and F. Plestan, "Asymptotically stable walking for biped robots: analysis via systems with impulse effects," *IEEE Transactions on Automatic Control*, vol. 46, no. 1, pp. 51-64, 2001.

[20] C. L. Shih, J. W. Grizzle, and C. Chevallereau, "Asymptotically stable walking of a simple underactuated 3D bipedal robot," *Proc. of 33rd Annual Conference of the IEEE Industrial Electronics Society (IECON)*, Taiwan, 2007.

[21] C. Chevallereau and J. W. Grizzle, "Asymptotically stable walking of a five-link underactuated 3-D bipedal robot," *IEEE Transactions on Robotics*, vol. 25, no. 1, pp. 37-50, 2009.

[22] M. Y. Cheng and C. S. Lin, "Measurement of robustness for biped locomotion using linearized Poincaré map," *Proc. of IEEE International Conference on Intelligent Systems, Man and Cybernetics*, Vancouver, Canada, 1995.

[23] C. Y. A. Chan, *Dynamic Modeling, Control and Simulation of a Planar Five-link Bipedal Walking System*, Master Thesis, Department of mechanical and Manufacturing Engineering, University of Manitoba, Canada, 2000.

[24] J. Liu, *Radial Basis Function (RBF) Neural Network Control for Mechanical Systems*, First edition, Springer, 2013.

[25] F. Allgower, and A. Zheng, *Nonlinear Model Predictive Control, Birkhauser*, Beilin Germany, 2000.

[26] S. Wiggins, *Introduction to Nonlinear Dynamical Systems and Chaos*, 2nd Edition, Springer Verlag, New York, 2000.

[27] S. H. Hyon and T. Emura, "Symmetric walking control: Invariance and global stability," *Proc. of IEEE International Conference on Robotics and Automation*, pp. 1455-1462, Barcelona, Spain, 2005.

[28] R. Fletcher, *Practical Methods of Optimization*, John Wiley & Sons, New York, 1987.

Reza Heydari received his B.S. degree from Sahand University of Technology, Tabriz, Iran, in 2011, and M.Sc degree from Iran University of Science and Technology, Tehran, Iran, in 2014, His research interests include model predictive control, bipedal walking, intelligent control, system identification and control algorithm.

Mohammad Farrokhi has received his B.S. degree from K.N. Toosi University, Tehran, Iran, in 1985, and his M.S. and Ph.D. degrees from Syracuse University, Syracuse, New York, in 1989 and 1996, respectively, all in Electrical Engineering. He joined Iran University of Science and Technology in 1996, where he is currently an Associate Professor of Electrical Engineering. His research interests include automatic control, fuzzy systems, and neural networks.